RSC Advances

PAPER

View Article Online
View Journal | View Issue

Cite this: *RSC Adv.*, 2020, **10**, 3978

A novel nanoparticle loaded with methyl caffeate and caffeic acid phenethyl ester against *Ralstonia solanacearum*—a plant pathogenic bacteria†

Jin-Zheng Wang,‡[a] Cheng-Hai Yan,‡[a] Xiao-Rui Zhang,[a] Qing-Bo Tu,[a] Yan Xu,[abcd] Sheng Sheng,[abcd] Fu-An Wu[abcd] and Jun Wang *[abcd]

Developing a novel agent and understanding the interaction model between multipolymer nanoparticles and bacteria could be worthwhile to induce the protection of crops with the prevalence of frequent hazards because of the use of pesticides and chemical resistance. Unlike metal nanoparticles, multipolymer nanoparticles have bacteriostatic properties against *Ralstonia solanacearum* that can trigger bacterial wilt by infecting the plant. Therefore, a novel poly(lactic-*co*-glycolic acid) nanoparticle containing caffeic acid phenethyl ester (CAPE) and methyl caffeate (MC) was prepared with the sustained-release property (for 10 d at pH 6.5); here, 50% of the cumulative release rate was achieved. It was observed that the cytomembrane of *R. solanacearum* was jeopardized by the nanoparticle by the creation of large holes on the bacterial surface. The nanoparticle has an approximate EC_{50} value of 0.285 mg mL^{-1} with active pharmaceutical ingredients (APIs), while the drug dosage could be reduced by 2/3. Furthermore, to reveal the possible mechanism of interaction between the multipolymer nanoparticles and bacteria, a formidable inhibition effect was observed; the pathogenicity-related genes, namely, *phcA*, *phcB*, *pehC*, *egl*, *pilT*, and *polA*, of *R. solanacearum* were downregulated by 1/2, 1/42, 1/13, 1/6, 1/2, and 1/8, respectively, showing significant effects on the major virulence-related genes. Hence, a novel nanoparticle with excellent antibacterial and sustained-release properties has been prepared, possessing the potential to replace chemical pesticides and serve as a new control strategy for mulberry blight disease.

Received 13th November 2019
Accepted 24th December 2019

DOI: 10.1039/c9ra09441e

rsc.li/rsc-advances

1. Introduction

The benefits of worldwide pesticide utilization have become limited due to their effects on the environment.[1] Due to the long-term effect of chemical pesticides, the efficiency of pesticide control has weakened. Many pesticide residues have become ubiquitous in the natural environment and are present ranging from nanogram per liter to low milligram per liter concentrations, which can cause serious microbial species balance,[2] soil microenvironment change,[3] and effects on human health.[4] In particular, during the study on the control strategy of bacterial wilt disease caused by *Ralstonia solanacearum*, which is one of the most harmful soil-borne diseases in the world due to its wide distribution and host range,[5] traditional chemical pesticides and antibiotics have been employed against *R. solanacearum* despite issues such as limited efficacy, microbial resistance strains, environmental pollution, and potential health risks to human health.[6] Therefore, it has become urgent to develop an alternative agent without any collateral damage to replace traditional chemical pesticides and protect economic crops from plant pathogens such as *R. solanacearum*.

In the development of antibacterial agents, polymeric nanoparticles have been considered as novel antibacterial agents with the ability to enhance the antibacterial properties.[7] Poly-(lactic-*co*-glycolic acid) (PLGA), a novel material for preparing polymeric nanoparticles, has been commonly used as the polymer material in drug delivery systems. Generally, PLGA nanoparticles have a sustained-release capacity,[8] which has very environmentally friendly properties; this occurs because of the hydrolysis of ester bonds in water to form lactic acid and glycolic acid.[9] Further, this release capacity might lead to an incomplete release, which can cause several active pharmaceutical ingredients (APIs) to directly exist in the soil after PLGA

[a]*School of Biotechnology, Jiangsu University of Science and Technology, Zhenjiang 212018, PR China. E-mail: wangjun@just.edu.cn; Fax: +86-511-85620901; Tel: +86-511-85635867*

[b]*Sericultural Research Institute, Chinese Academy of Agricultural Sciences, Zhenjiang 212018, PR China*

[c]*Key Laboratory of Silkworm and Mulberry Genetic Improvement, Ministry of Agriculture and Rural Affairs, Zhenjiang 212018, PR China*

[d]*Jiangsu Key Laboratory of Sericultural Biology and Biotechnology, Zhenjiang 212018, PR China*

† Electronic supplementary information (ESI) available. See DOI: 10.1039/c9ra09441e

‡ These authors contributed equally to this work.

degradation. The modification of the nanoparticle surface, such as the application of antibodies,[10] might be helpful to resolve this problem. In addition, nanoparticles prepared with PLGA can improve the solubility and dispersibility of nanoparticles in water without affecting their efficacy.[11] Furthermore, polymeric nanoparticles have been considered to be the most promising approach against drug resistance of bacteria.[12,13] Nanoparticles can be used as alternative tools to handle drug-resistant pathogens.[14] Hence, nanoparticles prepared with PLGA have the potential to be an alternative to traditional pesticides.

Due to the ability of *R. solanacearum* to maintain its activity in soils for a long period of time[15] and its complex genetic regulatory system, it is difficult to eradicate this bacterium by means of chemical pesticides and antibiotics, even those that cause serious environmental issues. Nearly 30 provinces in China have suffered from problems related to *R. solanacearum*, and mulberry trees in Jiangsu and Zhejiang provinces, as well as potatoes in Fujian province, have been afflicted with the most serious damage.[16] As early as 2012, *R. solanacearum* was ranked as the second most harmful plant pathogen in the top 10 bacterial plant pathogens.[17] In addition, because *R. solanacearum* can enter through the plant roots, invade xylem vessels, and rapidly spread to the aerial parts of the plant,[15] the swimming motility of *R. solanacearum* can facilitate its ability to infect plants. Furthermore, the expression of virulence factors also plays a crucial role in the pathogenesis of *R. solanacearum*. The virulence of filamentous phage against *R. solanacearum* was evaluated by detecting the expression of pathogenicity-related genes in *R. solanacearum* (physiological race 1, biochemical type 3), and open reading frame (ORF) 15 of φRSM phage can inhibit the transcriptional regulator *phcA*, causing pathogenicity in the phenotypic transformation system of *R. solanacearum*, which can reduce pathogenicity.[18] Further, considering the complex regulatory mechanism of *R. solanacearum*, the combination of multiple APIs might help to reduce the resistance of pathogenic bacteria toward agents.

Since antibiotics can lead to increased resistance of pathogenic bacteria, natural source agents and their derivatives have become the mainstays in the development of antibacterial agents.[19] Due to their potential ability to inhibit bacteria, our attention has been focused on caffeic acid—a naturally sourced compound—and its derivatives. Among them, caffeic acid phenethyl ester (CAPE), which is considered to be one of the most popular compounds for the development of new drugs[20] and has been the main active ingredient isolated from propolis residues, has shown toxic effects toward *R. solanacearum*.[21] Methyl caffeate (MC) has many pharmacological activities, and it is a synthetic intermediate of many natural drugs and food additives, such as propyl caffeate (PC); CAPE can be prepared by the transesterification of MC with the corresponding alcohol.[22] Recently, PLGA particles loaded with CAPE were successfully prepared,[20] which demonstrated the feasibility of fabricating PLGA particles loaded with caffeic acid and its derivatives. Many studies have focused on the preparation process as well as the lack of research on the mechanism of bacteriostatic action of the prepared nanoparticles. Therefore, a brief description of the possible bacteriostatic mechanisms has been provided in this study. Further, MC and CAPE were employed as a combination of APIs to develop an alternative agent for controlling plant pathogens, and the preparation of PLGA nanoparticles loaded with MC and CAPE can hopefully become an alternative agent with high efficiency and low toxicity.

In this study, an emulsion solvent evaporation technique was employed to prepare PLGA nanoparticles loaded with MC and CAPE, while the drug loading rate (DL) was selected as the main evaluation standard. Parameters such as polyvinyl alcohol (PVA) concentration, ultrasonic power, ultrasonic time, and ratio of the organic phase to aqueous phase were optimized. The slow-release characteristics of these novel nanoparticles were also investigated. To investigate the antibacterial activity of the nanoparticles on *R. solanacearum*, RT-PCR was employed to detect the expression levels of pathogenicity-related genes, and scanning electron microscopy (SEM) was employed to observe the treated strains. Susceptibility testing by the disk diffusion method of the nanoparticles was also carried out to preliminarily evaluate the drug resistance after treatment.

2. Experiment method and material

2.1 Experimental materials and strains

Tryptone LP0042 was purchased from Oxoid, UK. Casein hydrolysate, PLGA (lactide : glycolide = 50 : 50; intrinsic viscosity: 0.45–0.60 dL g^{-1}; M_w: ~38–54 kDa P50/50), and PVA 124 (viscosity: 40 g L^{-1}, 20 °C, 54.0–66.0 (mPa s)$^{-1}$) were purchased from Sigma-Aldrich (St. Louis, MO, USA). Caffeate derivatives such as MC and CAPE were prepared by our group.[21,23] SYBR premix Ex Tap™ II (Tli RNaseH Plus), primer script RT reagent kit with gDNA eraser (Perfect Real Time), DEPC water, and isopropanol were purchased from Takara. The total RNA extraction reagent TRIzol and PCR kit were purchased from Sangon Biotech. RS-5 *R. solanacearum* strains were used, which were isolated from mulberry roots.[21] All the primers were synthesized by Shanghai Biotech; the primer sequences were synthesized as described elsewhere,[18] as listed in Table 1.

2.2 Preparation of nanoparticles loaded with CAPE and MC

The preparation of nanoparticles by a single emulsion/solvent evaporation method was based on other studies.[11] The effects of PVA concentration, ultrasonic power, ultrasonic time, and ratio of the organic phase to aqueous phase on nanoparticle preparation were investigated. In the first stage, 100 mg PLGA and 55 mg API (MC and CAPE at a mass ratio of 1 : 1) were dissolved in 1.5 mL dichloromethane and 0.5 mL ethanol, respectively. After complete dissolution, the mixture was shaken for 5 min, completing the preparation of the organic phase. PVA (1%, 2%, 3%, 4%, 5%, and 10% w/w) was heated with deionized water in an ultrasonic water bath at 80 °C until dissolution to prepare the aqueous phase. After the second stage, the organic and aqueous phases were mixed according to various volume ratios (2 : 3, 1 : 2, 2 : 5, and 1 : 3) in an ice bath and then subjected to ultrasonic treatment using a microtip probe sonicator (65, 130, 195, 260, 325, 390, 474.5, and 650 W; amplitude: 80%; 2, 4, 6, 8, and 10 min); the mixture

Table 1 Primer information of the pathogenicity-related genes of *R. solanacearum*[a]

Primer name	Nucleotide sequence (5′ → 3′)	Size (bp)
Egl3-F	CAGCGCGACCTACTACAAGA	299
Egl3-R	TCATCAGCCCGAAGATGAC	
PhcA(298)-F	GGACATGATCTTCACGGTCAACT	298
PhcA(298)-R	GACTCATCCTCCTTTTCTGCATC	
PhcB(RT)-F	CTACCAGATCGTCGTCAATGAA	172
PhcB(RT)-R	GTCGAGGTAGTGCTTGATCTTG	
HrpB(RT)-F	TTCTCGATGATGTAGCGATAGG	238
HrpB(RT)-R	GCTGGAATTTTCGACTTCCTCTA	
PehC(RT)-F	GTTGTTCGGATTGCTGTACG	227
PehC(RT)-R	AGTCAAACGATTGCCTGAACTA	
PilT(175)-F	AAGAACAAAGCGTCTGATCTGC	175
PilT(175)-R	CTTCCAGGTTTTCTTCGTAATGCT	
polA-238F	GGAATGTCGGAAAGTCAAGAAA	238
polA-238R	CTTGTAGGCGGGGTACAGTTC	
16SrRNA349-F	CTAGAGTGTGTCAGAGGGAGGTAGA	349
16SrRNA349-R	ATGTCAAGGGTAGGTAAGGTTTTTC	

[a] F represents the leading chain and R represents the trailing chain.

was stirred overnight under magnetic force at room temperature. Thereafter, the obtained white emulsion was centrifuged 3 times at 3000 rpm to remove the precipitate; then, the remaining solution was centrifuged 3 times at 12 000 rpm for 40 min to obtain the precipitate. The supernatant was discarded. Finally, a small amount of deionized water was added to resuspend the precipitate. The mixture was then lyophilized for 48 h, and the lyophilized nanoparticles were stored in a freezer at −80 °C.

2.3 Determination of DL and encapsulation efficiency (EE) of the nanoparticles

The nanoparticles were dissolved in methanol at a mass-to-volume ratio of 2 : 1. To determine the MC and CAPE concentrations, the nanoparticle structures were destroyed by ultrasonication at room temperature for 30 min. The total amount of drug substrate in the nanoparticles was determined by high-performance liquid chromatography (HPLC) according to the standard curves of MC and CAPE, and the EE and DL values of the nanoparticles were calculated as follows:

$$\mathrm{EE}(\%) = \frac{W_1}{W_2} \times 100\% \quad (1)$$

$$\mathrm{DL}(\%) = \frac{W_1}{W_3} \times 100\% \quad (2)$$

W_1 represents the amount of drug (mg) encapsulated in the nanoparticle; W_2 represents the total dose (mg) of the input; and W_3 represents the total mass (mg) of the nanoparticle. The standard curve formulas of MC and CAPE are shown in eqn (3) and (4), and the measurement methods were carried out in accordance with an earlier research.[21]

$$\text{MC standard curve line: } Y = 5.64 \times 10^7 \times X - 2.35 \times 10^5, \quad R^2 = 0.9914 \quad (3)$$

$$\text{CAPE standard curve line: } Y = 5.48 \times 10^7 \times X - 2.33 \times 10^5, \quad R^2 = 0.9908 \quad (4)$$

2.4 FTIR characterization of nanoparticles

Ultraviolet-visible near-infrared absorption spectrometry was employed to reconfirm the presence of MC and CAPE in the nanoparticles.[24] Each sample was scanned 10 times, in the range of 4000–750 cm^{-1} at a resolution of 4 cm^{-1}.

2.5 Drug release characteristics of nanoparticles

The determination of sustained-release kinetics was based on an earlier reported method[20] with slight modifications. Nanoparticles and phosphate-buffered solution (pH 7.4, 6.5, and 9.5) were mixed at a solid–liquid ratio of 2 : 1. The mixtures were incubated at 37 °C under shaking and sampled at designated time intervals (1, 2, 3, 4, 5, 6, 9, 12, 15, 24, 27, and 30 h after incubation). The release medium was centrifuged at 9000 rpm for 3 min. The supernatant was collected and the solution was replaced with fresh PBS for continued incubation. The collected samples were lyophilized and dissolved in 1 mL methanol solution. Thereafter, HPLC was employed to detect the MC and CAPE concentrations, and the method was performed according to an earlier research.[21] The Fickian diffusion model[25] was used to evaluate the release process of polymer nanoparticles; the release mechanism was described by a semiempirical eqn (5).

$$\frac{M_x}{M_\infty} = kx^n + \alpha \quad (5)$$

M_x represents the mass of the drug released at time x; M_∞ refers to the mass of the drug released at infinite time; k stands for the kinetic constant; n stands for a constant; further, the geometry of the nanoparticles and release mechanism is related.

2.6 SEM of *R. solanacearum*

Antibacterial treatment was carried out according to an earlier research.[21] Gemini SEM 300 (ZEISS, Germany) was employed to evaluate the morphology of *R. solanacearum*, and the inhibitory effect of bacteriostatic agents was evaluated by observing the changes in the cell membrane and cell morphology.

2.7 Antibacterial rate of nanoparticles against *R. solanacearum*

The antibacterial activity of nanoparticles was determined according to an earlier research[26] with slight modifications. Different concentrations of nanoparticles (4, 3.2, 1.6, 0.8, 0.4, 0.2, and 0.1 mg mL^{-1}) were added to the wells of a 96-well plate. A microplate reader (SpectraMax i3, Silicon Valley, CA, USA) was used to determine the optical density of the plates at 600 nm at T0 before incubation. The OD_{600} value was measured as the TF after the plates were incubated at 30 °C overnight under shaking for 5 min. The antibacterial rate of the nanoparticles against *R. solanacearum* was calculated according to eqn (6), and the EC_{50} calculation method was used according to the reported methods.[27]

$$\text{Inhibition}(\%) = \left(1 - \frac{\text{TF}_{\text{sample}} - \text{T0}_{\text{sample}}}{\text{TF}_{\text{blank}} - \text{T0}_{\text{blank}}}\right) \times 100\% \quad (6)$$

$T0_{sample}$ and TF_{sample} indicate the OD_{600} values of the bacterial solution before and after the addition of nanoparticles, respectively. $T0_{blank}$ and TF_{blank} indicate the OD_{600} values of the control solution before and after incubation, respectively.

2.8 Pathogenicity-related gene expression of *R. solanacearum*

The nanoparticles (4 mg mL^{-1}), API (4 mg mL^{-1}), and Triton X-100 were added to the bacterial suspension (OD_{600} = 0.8–1) at a volume ratio of 2 : 1 and incubated overnight at 30 °C for 24 h. After incubation, this treated bacterial suspension was separately centrifuged at 12 000 rpm for 3 min to collect the precipitates of different treatment strains. The total RNA extraction process was carried out according to the protocol modifications.[28] Briefly, the Trizol reagent (Invitrogen, USA) was used to extract the total RNA from each treatment sample and DNase I (Promega, Madison, WI, USA) was used to purify the total RNA. The prepared total RNA was stored at −80 °C. The PrimeScript RT Reagent Kit with gDNA Eraser (Takara Biotechnology, Otsu, Japan) was used to synthesize the cDNA, and the product was stored at −80 °C for immediate measurement.

A LightCycler 96 real-time PCR system (Roche, Switzerland) was used to determine the relative expression of pathogenicity-related genes. Each reaction system (20 μL) contained 10 μL of TB Green, 0.8 μL of the upstream primer, 0.8 μL of the downstream primer, 6.4 μL of RNase-free double-distilled water, and 2 μL of cDNA. The specific primers (Table 1) were synthesized by Sangon in Shanghai according to another research,[18] and the 16S rRNA of *R. solanacearum* was used as the internal control for RT-qPCR to normalize the gene expressions of the pathogenicity-related genes.

2.9 Significance level analysis

Significance level analysis and EC_{50} calculations were performed using the SPSS 22 software, and the mapping was performed using OriginPro 9.0 software. All the experiments had three sets of repetitions, and the result was reflected in the error bar in the figures. The letters on the column indicate the differences between the different treatment groups, the same letters indicate that the difference is not significant ($P > 0.05$), and completely different letters indicate significant differences ($P < 0.05$).

3. Results and discussion

3.1 Nanoparticle preparation

Fig. 1A shows the effects of PVA concentration on the DL and EE of nanoparticles. When the PVA concentration was between 10 and 100 mg mL^{-1}, the EE values of MC and CAPE increased with the concentration, reaching the highest value of 28.25 ± 0.17% at 40 mg mL; further, they decreased from 28.25 ± 0.17% to 19.09 ± 1.04% for PVA concentrations between 40 and 100 mg mL^{-1}. As an emulsifier, the PVA concentration could increase the EE of the drug molecule.[29] However, when the emulsifier concentration was considerably increased, the EE and DL of the nanoparticles could reduce.[30] When the PVA concentration was 50 mg mL^{-1}, the DL reached the highest value, *i.e.*, 18.70 ± 0.80%. In addition, when the PVA concentration exceeded 40 mg mL^{-1}, the viscosity of the emulsion solvent was too high, making it difficult to separate the nanoparticles; further, at 30 mg mL^{-1} PVA, the DL (16.46 ± 0.18%) was close to the highest value (18.70 ± 0.80%), and the EE (25.26 ± 0.27%) was relatively high. Therefore, the suitable PVA concentration was 30 mg mL^{-1}.

Fig. 1B shows the effect of ultrasonic power on the DL and EE of nanoparticles and the emulsification treatment was carried out in the ultrasonic power range of 65–650 W. When the power was raised from 65 to 325 W, both DL and EE increased. The higher ultrasonic power could facilitate the formation of a uniform stable emulsion droplet.[31] When the ultrasonic power was 260 W, the EE reached the maximum value of 21.71 ± 1.64%. Although the DL reached the highest value of 14.65 ± 1.03% under ultrasonic power of 325 W, the EE was 21.44 ± 1.51%. However, increasing the ultrasonic power could enhance cavitation, which could reduce the DL. When the power was increased from 325 to 650 W, both DL and EE decreased. The increase in ultrasonic power could reduce the particle size, while the excessive energy could increase flocculation,[32] which could cause this decrease. Therefore, the power condition for obtaining the maximum DL was taken as the optimal condition, and the optimal ultrasonic power condition was 325 W.

Fig. 1C shows the effect of ultrasonic time on the EE and DL values. When the ultrasonic time was 2–10 min, the DL value decreases from 20.54 ± 0.22% to 14.89 ± 2.26%, which indicates that a longer ultrasonic time leads to a decrease in DL. The reason for this decrease might be the long-term cavitation effect caused by ultrasound, which may cause an increase in the droplet sizes[33] and the destruction of the formed emulsified droplets, resulting in a decrease in drug content. Furthermore, excessive time has a marginal effect on the formation of emulsion droplets, which could prolong the reaction time.[34] This optimal treatment condition with the highest DL was the same as that reported in another research;[11] therefore, 2 min was chosen as the suitable ultrasonic time.

Fig. 1D shows the effect of the ratio of the organic phase to aqueous phase on the DL and EE values of the nanoparticles. When this ratio was 1 : 2, the maximum values of EE and DL were achieved, namely, 37.08 ± 0.04% and 28.33 ± 0.03%, respectively. This ratio might not be conducive toward the dispersion of emulsified droplets, while the added PVA concentration was too small. In contrast, the addition of an excessive amount of PVA could result in a decrease in the EE of the nanoparticles due to a reduction in the amount of drugs scattered in the organic phase.[35] In addition, this could lead to an increase in the possibility of dissolution of the drug under the action of ultrasound. Therefore, the optimum ratio of the

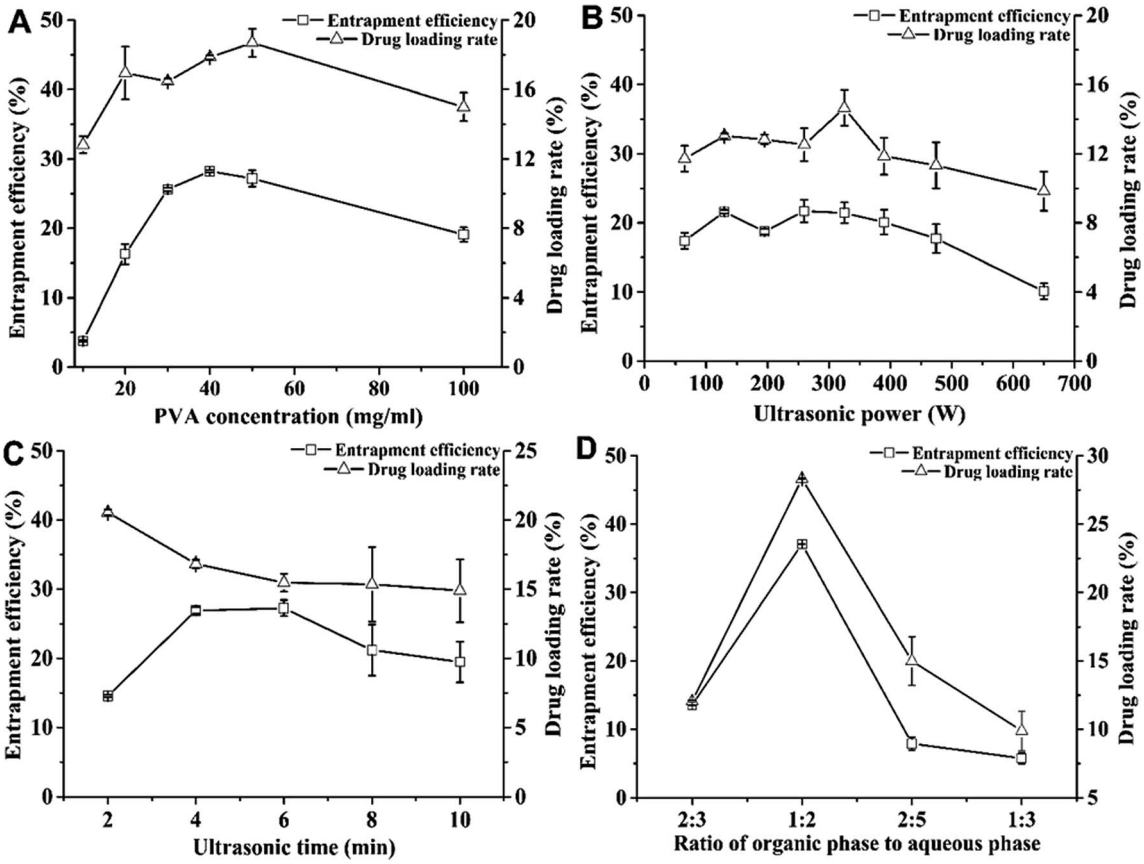

Fig. 1 Optimization of the preparation process of nanoparticles loaded with MC and CAPE. The effects of PVA concentration (A), ultrasonic power (B), ultrasonic time (C), and ratio of the organic phase to aqueous phase (D) on the drug loading rate and encapsulation efficiency of nanoparticles were investigated. Error bars represent the standard error of at least three independent trials.

organic phase to aqueous phase was selected to be 1 : 2, yielding the highest DL of 28.33 ± 0.03%.

Therefore, the optimum condition was as follows: 3% PVA with the ratio of organic phase to aqueous phase of 1 : 2 at 325 W under sonication for 2 min. Further, the highest DL (28.33 ± 0.03%) was achieved under this optimum condition.

3.2 Nanoparticle characterization

Fig. 2 shows the FTIR spectra of the nanoparticles, CAPE, MC, and PLGA, where 1763 cm^{-1} is the extension of the C=O bond in the ester bond and 1182–1095 cm^{-1} is the pull of the CO bond. These are the characteristic peaks of the PLGA molecules;[36] the main peaks of CAPE at 3478, 3323, and 1600 cm^{-1} were significantly reduced, indicating that CAPE was successfully embedded in the PLGA.[20] The hydroxyl group at 3478 cm^{-1} was stretched; the 1607, 1535, and 1445 cm^{-1} peaks denote the C=C bond stretching of the aromatic compound; and the 1307 cm^{-1} peak denoted the CO bond of –COOH. These are the characteristic peaks of MC.[37] In the nanoparticle spectra, the characteristic peaks, namely, 1281, 1307, 1607, 1535, and 1445 cm^{-1}, were significantly reduced, indicating that MC was successfully embedded in the PLGA. Hence, MC and CAPE were successfully embedded.

Fig. 3 shows the results of the particle size analysis and electron micrographs of the nanoparticles loaded with MC and CAPE. The particle size distribution is shown in Fig. 3A.

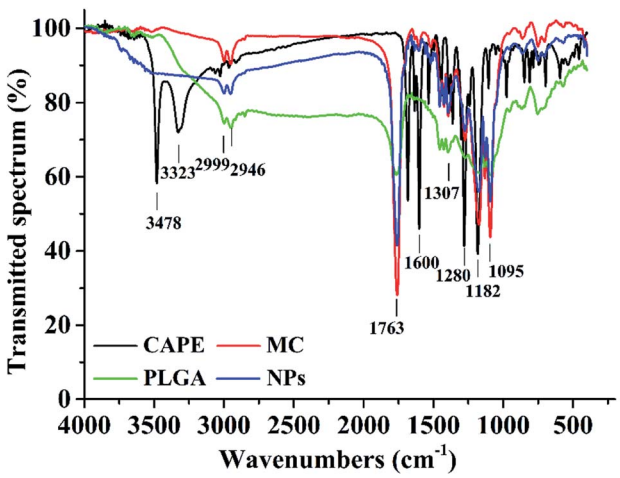

Fig. 2 Fourier-transform infrared spectra of the nanoparticles loaded with MC and CAPE (NPs). The nanoparticles were prepared under 3% PVA, ratio of the organic phase to aqueous phase of 1 : 2, and sonication power of 325 W for 2 min.

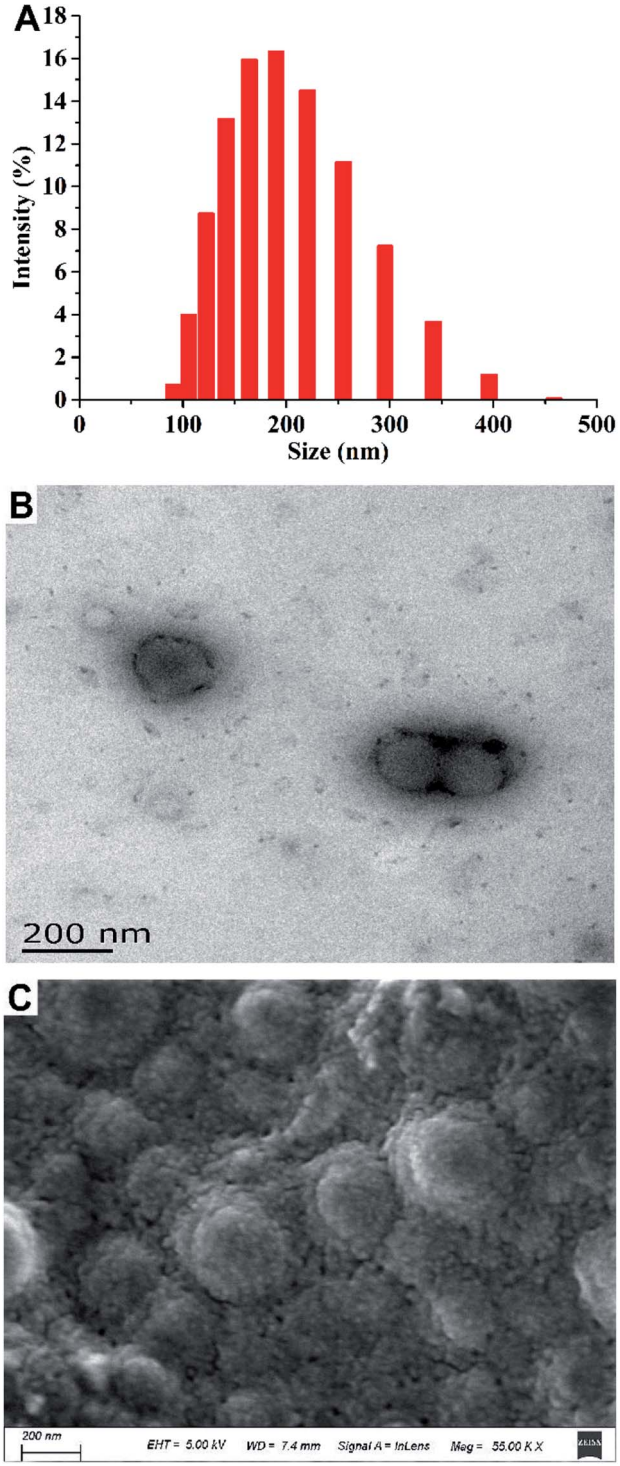

Fig. 3 Particle size analysis and electron micrographs of nanoparticles loaded with MC and CAPE. (A) The particle size distribution of nanoparticles loaded with MC and CAPE suspended in pure water. (B) Transmission electron microscopy image of nanoparticles loaded with MC and CAPE. (C) Scanning electron micrograph of nanoparticles loaded with MC and CAPE.

Particles with sizes below 200 nm accounted for 58.88%, whereas particles with sizes within 200–458 nm accounted for 37.80% of the total. The hydrated particle size was 188.86 nm. Fig. 3B shows the transmission electron microscopy image of the nanoparticles after reconstitution. The particle size range was 173.78–104.56 nm, and the results were consistent with the particle size analysis results. Fig. 3C shows the SEM image of a nanoparticle sample after lyophilization. The particle size was generally uniform, but the surface of the particle was rough due to lyophilization. In summary, the average particle size of the composite nanoparticles was 188.86 nm, and the particle shape was regular.

3.3 Release kinetics of the nanoparticle

In general, the drug release process of the nanoparticles comprised three stages. Fig. 4A shows that during the first stage (0–5 h) of the release process (called the initial burst release stage[11] with the highest rate), the drug molecules were adsorbed and were located adjacent to the surface of the nanoparticles that were first freely diffused into the solvent.[20] The cumulative release rate of the drug in the three buffers reached 16.75 ± 1.11% (pH 6.5), 15.34 ± 0.22% (pH 7.4), and 16.54 ± 0.56 (pH 9.5). The second stage (13–50 h) is the release stage in which the diffusion of the drug molecule and PLGA disintegration of the polymer material coexist. During this stage, the fixed drug molecules were released together, and the drug release rate significantly decreased when compared with the first stage. The cumulative release rates of the drug in the three buffers reached 26.56 ± 1.15% (pH 6.5), 26.13 ± 0.17% (pH 7.4), and 29.42 ± 0.42% (pH 9.5). During the third stage, the polymer began to disintegrate, releasing the drug molecules during disintegration; the release rate indefinitely reached zero, eventually entering a nearly linear sustained-release state.[11] In theory, there should also be a fourth stage,[25] where the remaining PLGA polymer containing the drug molecule rapidly disintegrates and releases the last drug molecule at a higher release rate, but this was not apparent due to the limited time.

The Fickian model was employed to formulate the delayed-release kinetic equations of the nanoparticles at pH 6.5, 7.4, and 9.5, which were termed as eqn (7), (8), and (9), respectively. Table 2 lists the results of the theoretical time required to reach 90% release rate and theoretical half-life of the nanoparticles calculated *via* the semiempirical formula. Under acidic conditions at pH 6.5, the release rate of the agent was lower, the theoretical half-life was approximately 10.0 d, and the theoretical time required for 90% drug release was approximately 44.1 d. The half-life at pH 9.5 and the theoretical time required to achieve a 90% drug release rate were 5.7 and 22.2 d, respectively. The higher pH might lead to the faster degradation of PLGA nanoparticles;[9] further, the alkaline environment accelerated the release of drug molecules in the nanoparticles, while the acidic environment slowed down the release of drug molecules. The pH in the mulberry soil was mostly acidic, which was beneficial to the long-term efficacy of nanoparticles in mulberry soil.

$$\frac{M_x}{M_{\infty\,\mathrm{pH=6.4}}} = 4.24 \times x^{0.43} + 5.27, R^2 = 0.8978 \quad (7)$$

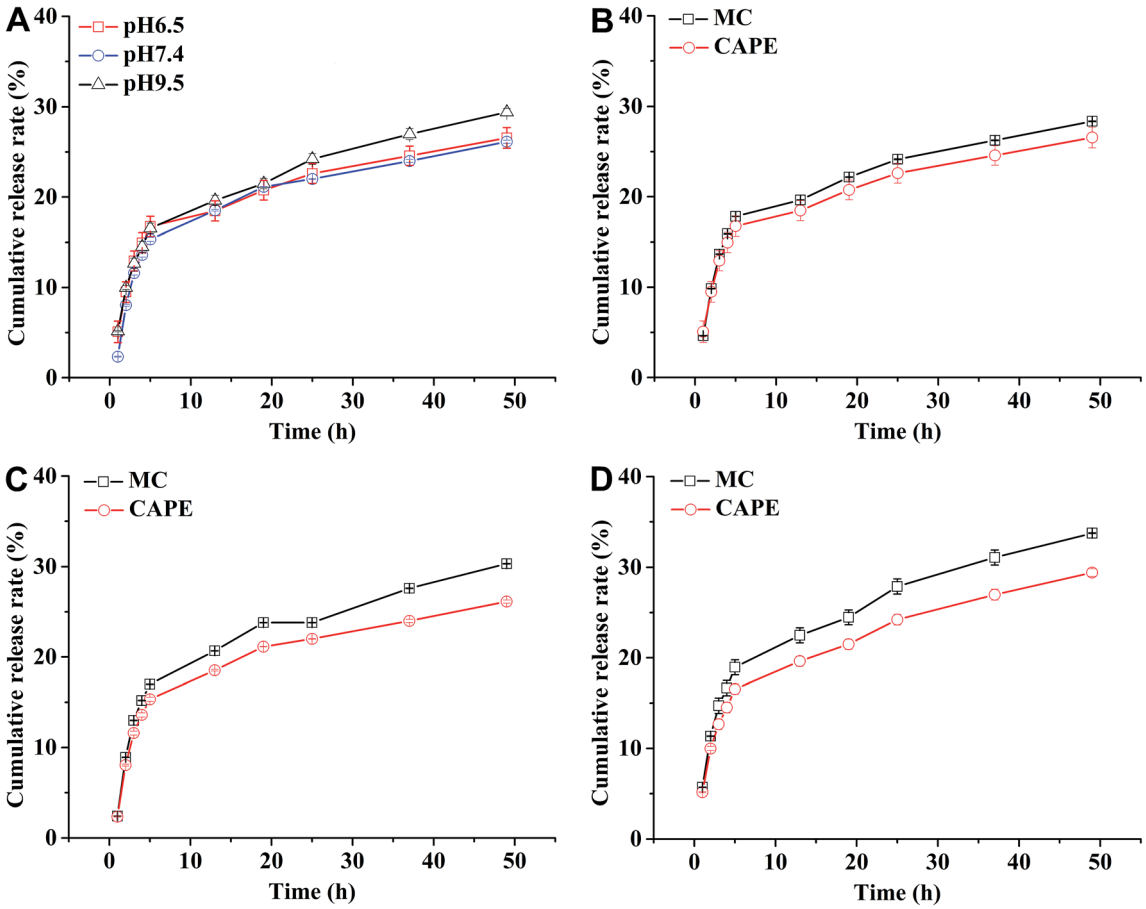

Fig. 4 Drug release profile of nanoparticles loaded with MC and CAPE (A) and release curves of MC and CAPE contained in this nanoparticle at pH 6.5 (B), pH 7.4 (C), and pH 9.5 (D). The nanoparticles loaded with MC and CAPE were prepared under 3% PVA with a ratio of the organic phase to aqueous phase of 1 : 2 at 325 W under sonication for 2 min. Error bars represent the standard error of at least three independent trials.

$$\frac{M_x}{M_{\infty\,\mathrm{pH=7.4}}} = 6.23 \times x^{0.43} - 1.85, R^2 = 0.9398 \quad (8)$$

$$\frac{M_x}{M_{\infty\,\mathrm{pH=9.5}}} = 6.10 \times x^{0.43} - 0.65, R^2 = 0.9456 \quad (9)$$

The nanoparticles in the acidic buffer were found to have a long half-life with a theoretical value of 10.0 d. The theoretical time required to release 90% of the agent under this condition was 44.1 d, but there was a burst in drug release within 0–5 h.[11] The drug release rate under these three pH conditions was above 15%: the minimum value was 15.34 ± 0.22% (pH 7.4). This phenomenon was mainly caused by the excessive adsorption of drug molecules on the surface of the nanoparticles and adjacent surfaces. Therefore, the nanoparticles exhibited excellent sustained-release properties, and the half-life reached up to 10.0 d at pH 6.5.

Fig. 4B–D show the release curves of MC and CAPE at different pH values in the nanoparticles. The maximum cumulative release rates of MC (18.95 ± 0.82%) and CAPE (15.63 ± 2.27%) were achieved during the first stage under pH 9.5 and 6.5, respectively. After 13 h, the degradation stage of the PLGA particles was accompanied by the slow dissolution of MC and CAPE. At pH 9.5 and a release time of 50 h, the cumulative release rate of MC was 33.76 ± 0.01%, and the cumulative release rate of CAPE was 24.73 ± 0.64%. The cumulative release rates of MC were larger than those of CAPE at pH 6.5, 7.4, and 9.5. This phenomenon could be attributed to the different distributions of MC and CAPE during emulsification. The shorter alkyl chain of MC has a stronger affinity toward water than CAPE, which might result in different distributions during emulsification. The MC molecule adsorbed and embedded itself on the surface of PLGA nanoparticles more than that for CAPE. The release of the drug molecules adsorbed and embedded on the surface of the PLGA particles is faster,[38] resulting in the larger cumulative release rate of MC within the same period of time during the first two stages of drug release. Therefore, combined with the multiple actions of nanoparticles, the inhibitory effect of nanoparticles containing MC and CAPE on *R. solanacearum* not only complicates inducing drug resistance, but also has the effect of batch release of drug molecules on the cell membrane of *R. solanacearum*.

Table 2 Theoretical half-lives of the nanoparticles loaded with MC and CAPE and theoretical time required to reach 90% release rate

pH of buffer	Half-life (days)	Time to reach 90% release rate (days)
6.5	10.0	44.1
7.4	5.8	21.8
9.5	5.7	22.2

3.4 Electron micrographs of *R. solanacearum* after nanoparticle treatment

Fig. 5 shows the treatment of *R. solanacearum* with API and nanoparticles; morphological changes were observed by using SEM. Fig. 5A shows the morphology of *R. solanacearum*. It was found that the flagellar structure of the strains treated with API and nanoparticles was destroyed, while the untreated strains were unharmed and the flagella structure was clearly visible. Fig. 5B shows the observation of *R. solanacearum* strains treated with API alone. The rod shape of the bacterium was deformed, the shape of the strains was distorted, and the flagella were also damaged to some extent, but the cell surface was not obviously damaged. However, Fig. 5C shows many strains with damaged cell membranes and incomplete flagella. Further, a large circular cavity appeared on the surface of *R. solanacearum*, as shown in Fig. 5D, and the cell membrane structure was seriously damaged, which may be related to the perforation effect of nanoparticles on the cell membrane.[39] Furthermore, the size of this cavity was similar to the hydrated particle size (188.86 nm), which confirmed that the particle might be involved. It was reported that PLGA-embedded drug particles might have certain adhesion to the surface of *Candida albicans*,[40] which can explain the huge pores appearing on the surface of *R. solanacearum*, possibly due to the attachment of nanoparticles to the cell surface. The PLGA-embedded drug particles disintegrate and release a large number of drug molecules, which causes the formation of pores on the cell membrane. Therefore, the nanoparticle has a certain perforation effect on the membranes of *R. solanacearum*.

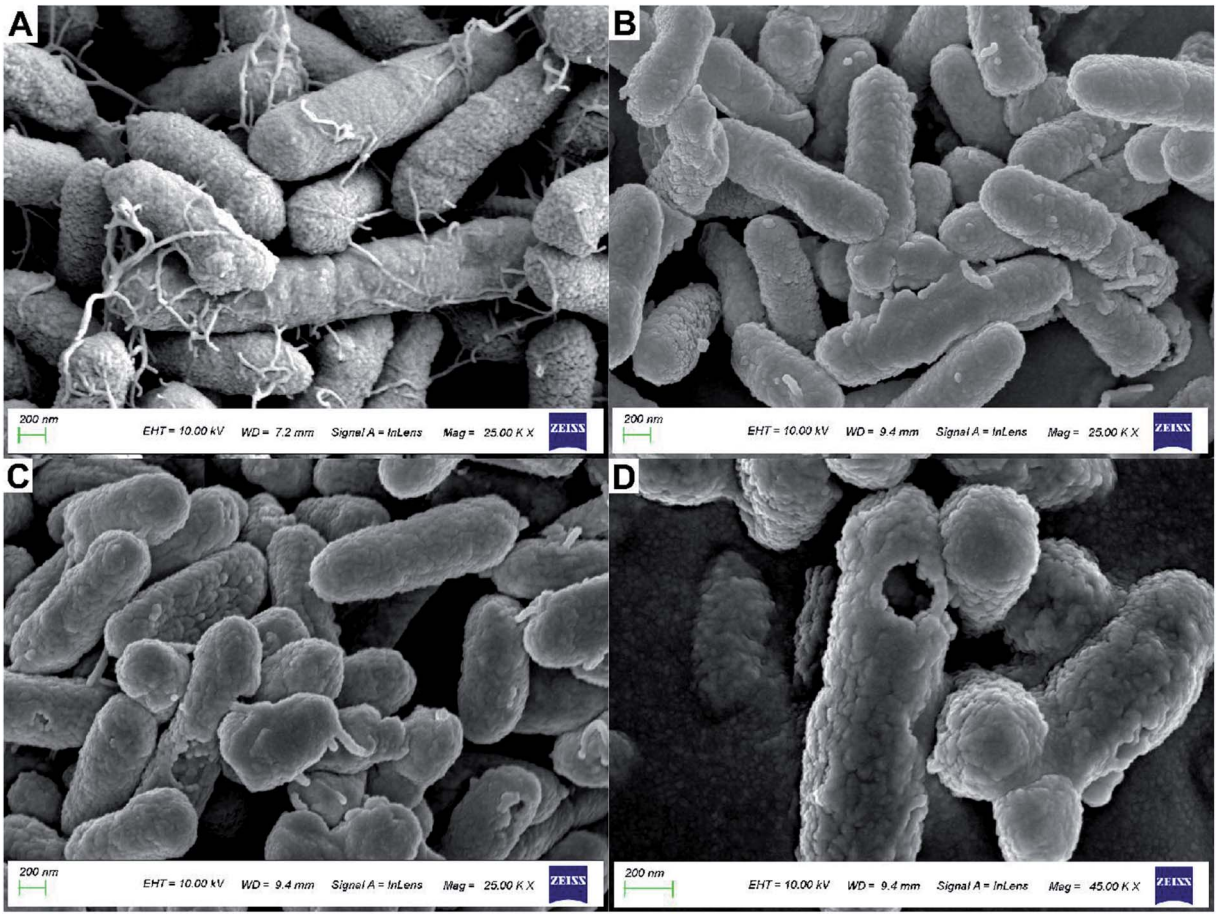

Fig. 5 Scanning electron micrographs of the bacteriostatic treatment of *R. solanacearum*. (A) The strains incubated at 30 °C for 24 h were designated as the blank control group with 2500k× magnification; (B) the strains treated with 4 mg mL^{-1} API were designated as the treatment group with 2500k× magnification; (C) the strains treated with 4 mg mL^{-1} nanoparticles loaded with MC and CAPE were designated as the treatment group with 2500k× magnification; (D) the strains treated with 4 mg mL^{-1} nanoparticles loaded with MC and CAPE were designated as the treatment group with 4500k× magnification.

Table 3 EC_{50} values of different dosages of antibacterial agents against *R. solanacearum* and the qualities of MC and CAPE required

Antibacterial agents	EC_{50} (mg mL^{-1})
MC	0.310
CAPE	0.165
APIs	0.248
Nanoparticles	0.285

3.5 Antibacterial activity of nanoparticles against *R. solanacearum*

Table 3 shows that under optimal conditions, the DL values of MC and CAPE in the nanoparticles were 14.50 ± 0.03% and 13.61 ± 0.27%, respectively. According to the literature,[27] the EC_{50} value of the nanoparticles was calculated to be 0.285 mg mL^{-1}. When a 50% inhibition rate was reached, the masses of MC and CAPE contained in 1 mL suspension containing the nanoparticle were 41.33 and 38.79 μg, respectively. Under the same bacteriostatic effect, the qualities of MC or CAPE alone were 7.5 and 4.3 times the masses of MC and CAPE in the nanoparticle, respectively, and the quality of the APIs was required to be 3 times that of the nanoparticle. Considering that the free bulk drug could facilitate the absorption of bacteria, its excellent efficacy needs to be based on the use of a higher amount of APIs, and the nanoparticle prepared in this study could considerably reduce the use of APIs, indicating its worthwhile technical economy. Furthermore, Fig. S1† shows the image of the susceptibility testing by the disk diffusion method. Evidently, the strains treated with the nanoparticles could not form visible plaques when compared with the other plates after incubation for 7 d. This phenomenon indicated that the novel nanoparticles loaded with MC and CAPE might possess the ability against the resistance of *R. solanacearum*, which could be supported by the data from recent studies according to which polymeric nanosystems might be a new prospect for treating multidrug-resistant bacteria.[13] Therefore, nanoparticles can effectively improve the antibacterial properties of caffeic acid esters in the aqueous phase with less API.

3.6 Expressions of pathogenicity-related genes during the early stage of infection after treatment

Fig. 6A shows the expression levels of *pehC*, *pilT*, and *polA* during the early stage of *R. solanacearum* infection. The expression levels of the polygalacturonase gene *pehC*[41] in the API and blank groups were 12.8 and 12.7 times than those in the nanoparticle group, respectively. The expression levels in the nanoparticle group were significantly lower than those in the other groups ($P < 0.05$). The expression of the *pilT* gene, which is a twitching motility-related gene,[42] also appeared to be inhibited, as shown in Fig. 6A; electron microscopy data confirmed that the number of bacterial flagella in the nanoparticle treatment group was significantly reduced. There was a significant difference in the expression levels in the nanoparticle and blank groups ($P < 0.05$). The expression levels of the blank and API groups were 2.3 and 1.6 times those of the nanoparticle group, respectively. In addition, the expression level of the DNA-polymerase-related gene *polA*[43] is shown in Fig. 6A. There was a significant difference among the four treatment groups ($P < 0.05$), where the nanoparticle group had the lowest expression level. The expression levels of the blank and API groups were 13.7 and 8.3 times those of the nanoparticle group, respectively. Therefore, the nanoparticles could inhibit the expressions of *pehC*, *pilT*, and *polA*.

3.7 Expressions of pathogenicity-related genes during the late infection stage after treatment

Fig. 6B shows the expression levels of *phcA*, *phcB*, and *egl*; *phcA* is the core regulatory gene of the phenotypic transformation system, which is the core system regulating the virulence and pathogenicity of the *R. solanacearum* infection[44] and regulates the expression of virulence factors such as EPS, plant cell wall-degrading enzymes, motility, and other regulatory elements.[45] As shown in Fig. 6B, the expression levels of *phcA* in the blank and API groups were 1.3 and 1.9 times those of the nanoparticle group, respectively. CAPE has a certain inhibitory effect on the various transcription factors (such as interleukin-6 and cyclooxygenase-2) and transcriptional activators in cells,[46] which may lead to the decreased expression of *phcA*. Further, the decreased expression of *phcA* might be one of the reasons for the decreased motility and the formation of a biofilm.[43] Furthermore, the *phcB* gene, which is involved in group signaling, was also inhibited, as shown in Fig. 6B. The expression of the *phcB* gene was significantly lower than those of the others ($P < 0.05$), resulting in the attenuation of the activation of the *phcA* expression,[47] which led to the downregulation of *phcA*. The expression of the *phcA* gene has a regulatory effect on the endoglucanase-related gene *egl*, confirming the results of the decrease in the expression level of *egl* (Fig. 6B). Fig. 6B shows that in the presence of nanoparticles, the expression level of *egl* was at least 0.54 ± 0.3, which was 1/2 that of the blank group; however, there was no significant difference between the blank and nanoparticle groups ($P > 0.05$). The above results reveal that the nanoparticles loaded with MC and CAPE have a certain inhibitory effect on the *egl*, *pehC*, *phcA*, *phcB*, *pilT*, and *polA* pathogenicity genes of *R. solanacearum*. The expression levels of *egl*, *pehC*, *phcA*, *phcB*, *pilT*, and *polA* were downregulated to 1/6, 1/13, 1/2, 1/42, 1/2, and 1/8 of that of the drug treatment group, respectively.

Fig. 7 shows the schematic diagram of the regulation of nanoparticles on some pathogenicity-related genes of *R. solanacearum*. When the nanoparticle was added to the bacterial suspension, the cell membrane and flagellum structure were severely damaged due to the multiple actions of the nanoparticles, which could be confirmed with the data shown in Fig. 5. The nanoparticles containing CAPE and MC continuously released CAPE and MC into the cells of *R. solanacearum*. The expression of *phcA*, an important regulatory factor in the phenotype transformation system, was inhibited; further, the expressions of the EGL and EPS phytotoxic factors were downregulated. In addition, in the detection of the pathogenicity-related genes of *R. solanacearum* before infecting the plants, it

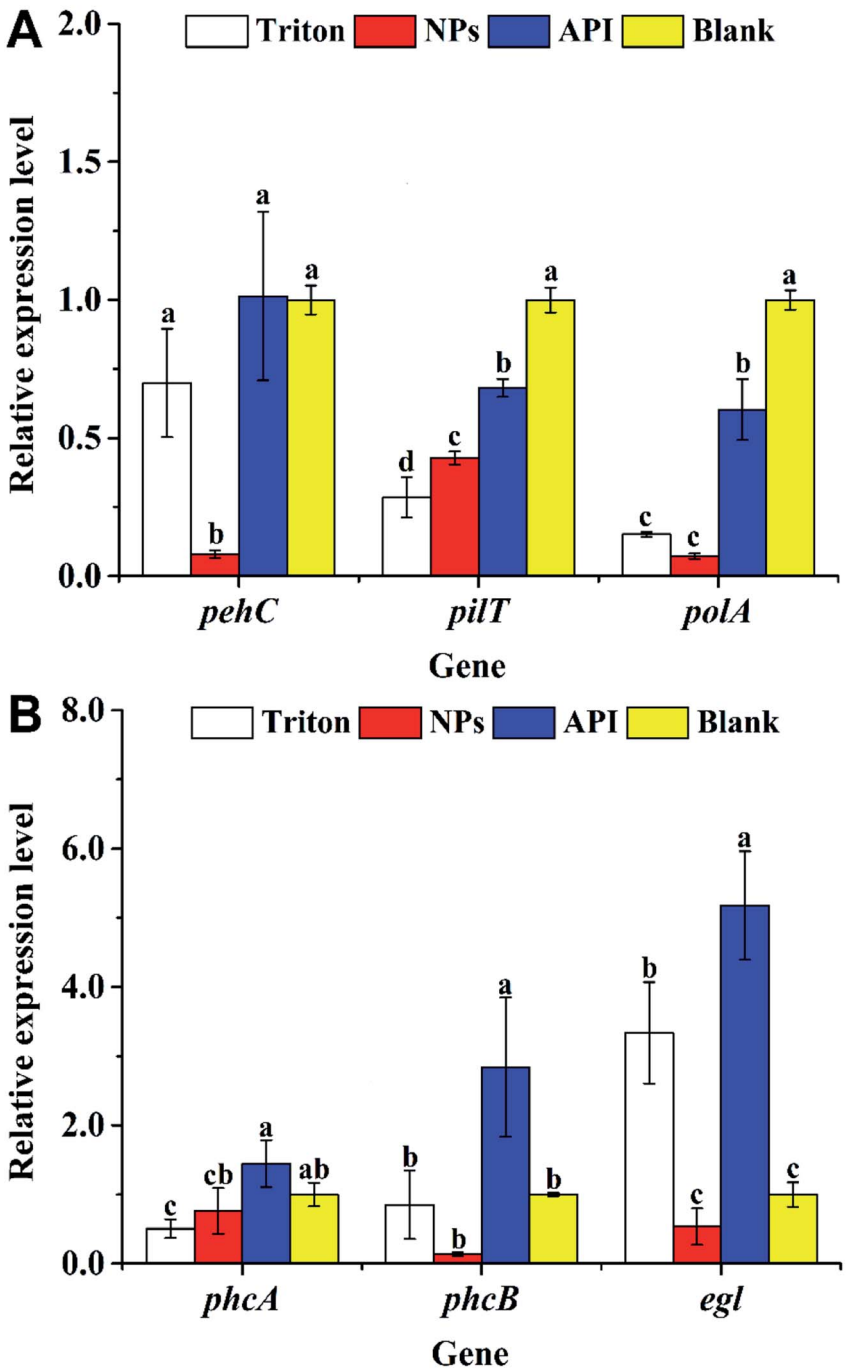

Fig. 6 Effect of nanoparticles loaded with MC and CAPE on the pathogenicity-related gene expression of *R. solanacearum*. Nanoparticles (4 mg mL^{-1}) loaded with MC and CAPE, 4 mg mL^{-1} active pharmaceutical ingredient, and Triton X-100 were added to the bacterial suspension (OD_{600} = 0.8–1) at a 2 : 1 volume ratio and incubated overnight at 30 °C for 24 h. These treatments were marked as NPs, API, and Triton groups, respectively. The untreated RS-5 bacterial suspension was set as the blank group. (A) The gene expression levels of *pehC*, *pilT*, and *polA* were obtained from *R. solanacearum* treated with the bacteriostatic agent for 24 h. (B) The gene expression levels of *phcA*, *phcB*, and *egl* were obtained from *R. solanacearum* treated with a bacteriostatic agent for 24 h. Error bars represent the standard error of at least three independent trials.

was found that the expression level of the transcriptional activator hrpB in the T3SS secretion system of *R. solanacearum* was extremely low to be used to calculate the relative expression. However, it has been reported that the expression of *hrpB* can be induced when *R. solanacearum* is cocultured with the plant suspension,[48] which might be the reason for the low expression of *hrpB*. In summary, the nanoparticles loaded with MC and CAPE have a certain inhibitory effect on the phenotypic

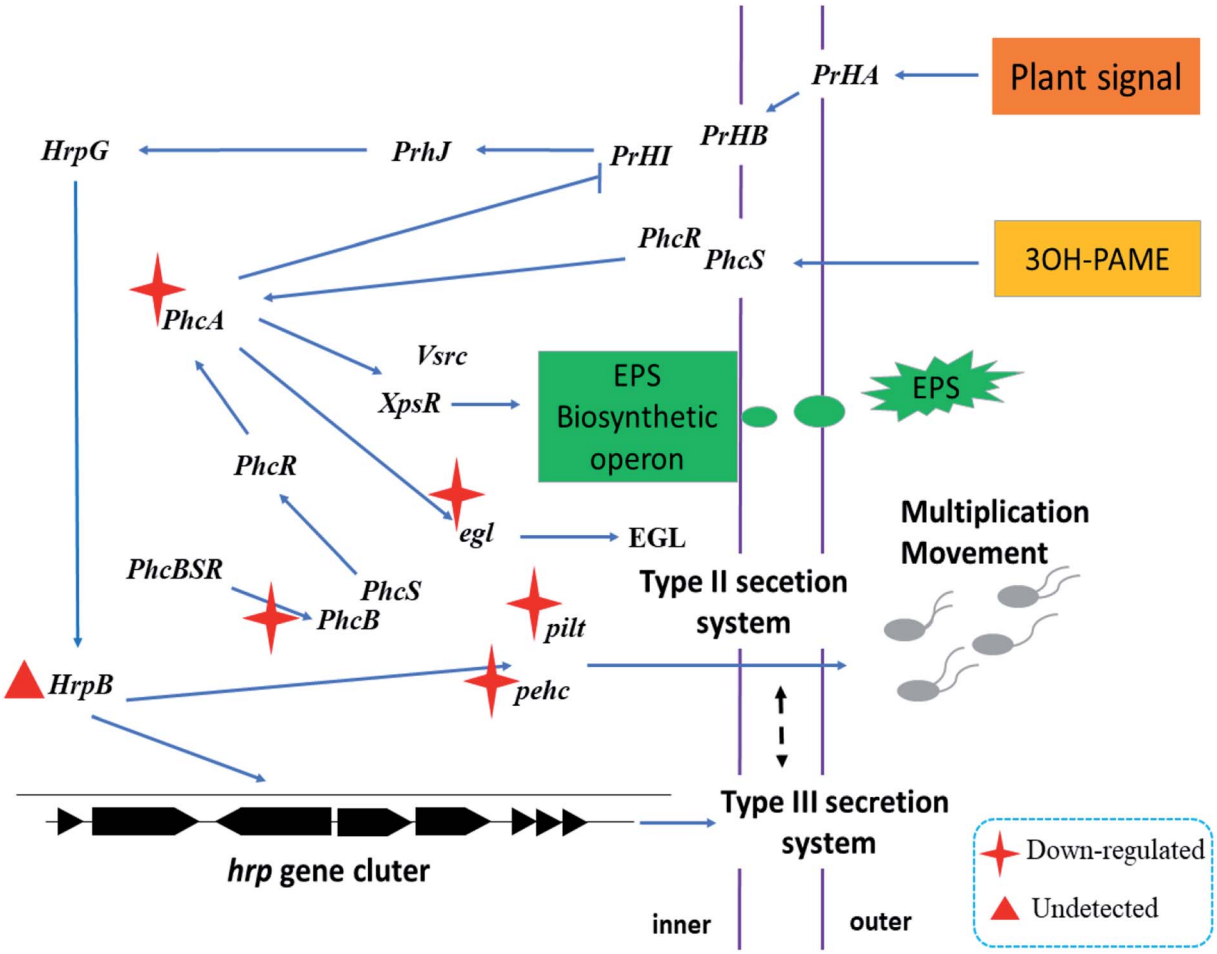

Fig. 7 Schematic of the regulation of nanoparticles loaded with MC and CAPE on some pathogenicity-related genes of *R. solanacearum*.

transformation system and the mobilization of *R. solanacearum*, and it is expected to develop into a new type of antibacterial agent.

4. Conclusions

In this paper, PLGA nanoparticles loaded with MC and CAPE were successfully prepared by a single emulsion/solvent evaporation method. The optimum conditions for obtaining the highest DL (28.33 ± 0.03%) were as follows: 3% PVA with a ratio of the organic phase to aqueous phase of 1 : 2 at 325 W under sonication for 2 min. Using the Fickian diffusion model to fit the sustained-release curve, the half-lives at pH 6.5, 7.4, and 9.5 were calculated to be 10.0, 5.8, and 5.7 d, respectively, indicating worthwhile sustained-release properties. The nanoparticles loaded with MC and CAPE were used for the antibacterial experiment of *R. solanacearum*, and the EC_{50} value was 0.285 mg mL^{-1}. Under the same antibacterial effect, the amount of nanoparticles used was 1/3 of the drug dose of API. The expression levels of the pathogenicity-related genes, namely, *egl*, *pehC*, *phcA*, *phcB*, *pilT*, and *polA*, of *R. solanacearum* were downregulated by RT-PCR to 1/6, 1/13, 1/2, 1/42, 1/2, and 1/8 of the drug-treated group, respectively, which have significant inhibitory effects on the major transcription factor *phcA* in the phenotype switching system. Therefore, the nanoparticles loaded with MC and CAPE show good sustained-release properties and good antibacterial effects, as observed by the disruption of the cytomembrane and suppression of pathogenicity-related gene expressions in *R. solanacearum*, which has the potential to be considered as a novel alternative agent for replacing traditional chemical pesticides.

Conflicts of interest

The authors have declared no conflicts of interest.

Acknowledgements

This study was financially supported by the Key Research and Development Program (Modern Agriculture) of Zhenjiang City (NY2017010), the National Modern Agricultural Industry Technology System of China (CARS-18-ZJ0305), the 333 High-level Talent Training Project of Jiangsu Province (BRA2019281), the Qing Lan Project of Jiangsu Province (Year of 2019), and the

Shen Lan Young scholars program of Jiangsu University of Science and Technology (Year 2015).

References

1 K. Fenner, S. Canonica, L. P. Wackett and M. Elsner, Evaluating pesticide degradation in the environment: Blind spots and emerging opportunities, *Science*, 2013, **341**, 752–758.

2 M. E. Delorenzo, G. I. Scott and P. E. Ross, Toxicity of pesticides to aquatic microorganisms: A review, *Environ. Toxicol. Chem.*, 2001, **20**, 84–89.

3 T. T. Iyaniwura, Non-target and environmental hazards of pesticides, *Rev. Environ. Health*, 1991, **9**, 161–176.

4 A. F. Hernandez, T. Parron, A. M. Tsatsakis, M. Requena, R. Alarcon and O. Lopez-Guarnido, Toxic effects of pesticide mixtures at a molecular level: Their relevance to human health, *Toxicology*, 2013, **307**, 136–145.

5 B. Kim, E. French, D. Caldwell, E. J. Harrington and A. S. Iyer-Pascuzzi, Bacterial wilt disease: Host resistance and pathogen virulence mechanisms, *Physiol. Mol. Plant Pathol.*, 2016, **95**, 37–43.

6 J. Chen, Y. Yu, S. Li and W. Ding, Resveratrol and coumarin: novel agricultural antibacterial agent against *Ralstonia solanacearum* in vitro and in vivo, *Molecules*, 2016, **21**, 1–18.

7 J. Chen, F. Wang, Q. Liu and J. Du, Antibacterial polymeric nanostructures for biomedical applications, *Chem. Commun.*, 2014, **50**, 14482–14493.

8 F. Danhier, E. Ansorena, J. M. Silva, R. Coco, A. Le Breton and V. Préat, PLGA-based nanoparticles: An overview of biomedical applications, *J. Controlled Release*, 2012, **161**, 505–522.

9 V. Singh, S. Singh, S. Das, A. Kumar, W. T. Self and S. Seal, A facile synthesis of PLGA encapsulated cerium oxide nanoparticles: release kinetics and biological activity, *Nanoscale*, 2012, **4**, 2597–2605.

10 C. Yang and D. Merlin, Can naturally occurring nanoparticle-based targeted drug delivery effectively treat inflammatory bowel disease?, *Expert Opin. Drug Delivery*, 2019, 1–4.

11 T. Arasoglu, S. Derman and B. Mansuroglu, Comparative evaluation of antibacterial activity of caffeic acid phenethyl ester and PLGA nanoparticle formulation by different methods, *Nanotechnology*, 2016, **27**, 25103.

12 R. Y. Pelgrift and A. J. Friedman, Nanotechnology as a therapeutic tool to combat microbial resistance, *Adv. Drug Delivery Rev.*, 2013, **65**, 1803–1815.

13 X. Ding, A. Wang, W. Tong and F. Xu, Biodegradable antibacterial polymeric nanosystems: A New hope to cope with multidrug-resistant bacteria, *Small*, 2019, **15**, 1900999.

14 B. Syed, M. N. N. Prasad, M. K. Kumar and S. Satish, Bioconjugated nano-bactericidal complex for potent activity against human and phytopathogens with concern of global drug resistant crisis, *Sci. Total Environ.*, 2018, **637**, 274–281.

15 G. Huet, Breeding for resistances to *Ralstonia solanacearum*, *Front. Plant Sci.*, 2014, **5**, 1–5.

16 G. Jiang, Z. Wei, J. Xu, H. Chen, Y. Zhang, X. She, A. P. Macho, W. Ding and B. Liao, Bacterial wilt in China: History, current status, and future perspectives, *Front. Plant Sci.*, 2017, **8**, 1–10.

17 J. Mansfield, S. Genin, S. Magori, V. Citovsky, M. Sriariyanum, P. Ronald, M. Dow, V. Verdier, S. V. Beer, M. A. Machado, I. Toth, G. Salmond and G. D. Foster, Top 10 plant pathogenic bacteria in molecular plant pathology, *Mol. Plant Pathol.*, 2012, **13**, 614–629.

18 H. S. Addy, A. Ahmed, K. Takeru, F. Makoto and Y. Takashi, Loss of virulence of the phytopathogen *Ralstonia solanacearum* through infection by φRSM filamentous phages, *Phytopathology*, 2012, **102**, 469–477.

19 G. D. Wright, Opportunities for natural products in 21st century antibiotic discovery, *Nat. Prod. Rep.*, 2017, **34**, 694–701.

20 S. Derman, Caffeic acid phenethyl ester loaded PLGA nanoparticles: Effect of various process parameters on reaction yield, encapsulation efficiency, and particle size, *J. Nanomater.*, 2015, **2015**, 1–12.

21 Y. Xu, S. Sheng, X. Liu, C. Wang, W. Xiao, J. Wang and F. A. Wu, Cooperative reinforcement of ionic liquid and reactive solvent on enzymatic synthesis of caffeic acid phenethyl ester as an in vitro inhibitor of plant pathogenic bacteria, *Molecules*, 2017, **22**, 72.

22 J. Wang, S. S. Gu, H. S. Cui, X. Y. Wu and F. A. Wu, A novel continuous flow biosynthesis of caffeic acid phenethyl ester from alkyl caffeate and phenethanol in a packed bed microreactor, *Bioresour. Technol.*, 2014, **158**, 39–47.

23 S. S. Wang, Z. J. Li, S. Sheng, F. A. Wu and J. Wang, Microfluidic biocatalysis enhances the esterification of caffeic acid and methanol under continuous-flow conditions, *J. Chem. Technol. Biotechnol.*, 2016, **91**, 555–562.

24 S. Derman, Z. A. Mustafaeva, E. S. Abamor, M. Bagirova and A. Allahverdiyev, Preparation, characterization and immunological evaluation: canine parvovirus synthetic peptide loaded PLGA nanoparticles, *J. Biomed. Sci.*, 2015, **22**, 89.

25 A. Budhian, S. J. Siegel and K. I. Winey, Controlling the in vitro release profiles for a system of haloperidol-loaded PLGA nanoparticles, *Int. J. Pharm.*, 2008, **346**, 151–159.

26 C. F. Yang, Y. Zhou, Y. Zheng, C. L. Li, S. Sheng, J. Wang and F. A. Wu, Enzymatic modification of chitosan by cinnamic acids: Antibacterial activity against *Ralstonia solanacearum*, *Int. J. Biol. Macromol.*, 2016, **87**, 577–585.

27 K. A. Nath, A. J. Croatt, S. Likely, T. W. Behrens and D. Warden, Renal oxidant injury and oxidant response induced by mercury, *Kidney Int.*, 1996, **50**, 1032–1043.

28 S. Sheng, C. W. Liao, Y. Zheng, Y. Zhou, Y. Xu, W. M. Song, P. He, J. Zhang and F. A. Wu, Candidate chemosensory genes identified in the endoparasitoid *Meteorus pulchricornis* (*Hymenoptera: Braconidae*) by antennal transcriptome analysis, *Comp. Biochem. Physiol., Part D: Genomics Proteomics*, 2017, **22**, 20–31.

29 A. Sahin, F. Spiroux, I. Guedon, F. B. Arslan, E. T. Sarcan, T. Ozkan, N. Colak, S. Yuksel, S. Ozdemir and B. Ozdemir, Using PVA and TPGS as combined emulsifier in

nanoprecipitation method improves characteristics and anticancer activity of ibuprofen loaded PLGA nanoparticles, *Pharmazie*, 2017, **72**, 525–528.

30 G. Gaucher, M. Poreba, F. Ravenelle and J. C. Leroux, Poly(N-vinyl-pyrrolidone)-block-poly(D,L-lactide) as polymeric emulsifier for the preparation of biodegradable nanoparticles, *J. Pharm. Sci.*, 2007, **96**, 1763–1775.

31 S. Freitas, G. Hielscher, H. P. Merkle and B. Gander, Continuous contact- and contamination-free ultrasonic emulsification—a useful tool for pharmaceutical development and production, *Ultrason. Sonochem.*, 2006, **13**, 76–85.

32 K. C. Guedes Silva and A. C. Kawazoe Sato, Sonication technique to produce emulsions: The impact of ultrasonic power and gelatin concentration, *Ultrason. Sonochem.*, 2019, **52**, 286–293.

33 S. M. M. Modarres-Gheisari, R. Gavagsaz-Ghoachani, M. Malaki, P. Safarpour and M. Zandi, Ultrasonic nano-emulsification – A review, *Ultrason. Sonochem.*, 2019, **52**, 88–105.

34 X. Luo, J. Cao, H. Yan, H. Gong, H. Yin and L. He, Study on separation characteristics of water in oil (W/O) emulsion under ultrasonic standing wave field, *Chem. Eng. Process.*, 2018, **123**, 214–220.

35 X. Song, Y. Zhao, S. Hou, F. Xu, R. Zhao, J. He, Z. Cai, Y. Li and Q. Chen, Dual agents loaded PLGA nanoparticles: Systematic study of particle size and drug entrapment efficiency, *Eur. J. Pharm. Biopharm.*, 2008, **69**, 445–453.

36 W. Hai, Z. Ying, W. Yan, H. Yu-Lin, N. Kaihui, N. Guangjun and C. Hao, Enhanced anti-tumor efficacy by co-delivery of doxorubicin and paclitaxel with amphiphilic methoxy PEG-PLGA copolymer nanoparticles, *Biomaterials*, 2011, **32**, 8281–8290.

37 M. K. Pyo, Y. Lee and H. S. Yun-Choi, Anti-platelet effect of the constituents isolated from the barks and fruits of *Magnolia obovata*, *Arch. Pharmacal Res.*, 2002, **25**, 325–328.

38 P. Rafiei and A. Haddadi, Docetaxel-loaded PLGA and PLGA-PEG nanoparticles for intravenous application: Pharmacokinetics and biodistribution profile, *Int. J. Nanomed.*, 2017, **12**, 935–947.

39 Y. J. Tang, J. M. Ashcroft, D. Chen, G. Min, C. Kim, B. Murkhejee, C. Larabell, J. D. Keasling and F. F. Chen, Charge-associated effects of fullerene derivatives on microbial structural integrity and central metabolism, *Nano Lett.*, 2007, **7**, 754–760.

40 L. Roque, N. Duarte, M. R. Bronze, C. Garcia, J. Alopaeus, J. Molpeceres, E. Hagesaether, I. Tho, P. Rijo and C. Reis, Development of a bioadhesive nanoformulation with *Glycyrrhiza glabra* L. extract against *Candida albicans*, *Biofouling*, 2018, **34**, 880–892.

41 E. T. Gonzalez and C. Allen, Characterization of a *Ralstonia solanacearum* operon required for polygalacturonate degradation and uptake of galacturonic acid, *Mol. Plant-Microbe Interact.*, 2003, **16**, 536–544.

42 N. Singh, T. Phukan, P. L. Sharma, K. Kabyashree, A. Barman, R. Kumar, R. V. Sonti, S. Genin and S. K. Ray, An innovative root inoculation method to study *Ralstonia solanacearum* pathogenicity in tomato seedlings, *Phytopathology*, 2018, **108**, 436–442.

43 W. Raza, J. Wang, Y. Wu, N. Ling, Z. Wei, Q. Huang and Q. Shen, Effects of volatile organic compounds produced by *Bacillus* amyloliquefaciens on the growth and virulence traits of tomato bacterial wilt pathogen *Ralstonia solanacearum*, *Appl. Microbiol. Biotechnol.*, 2016, **100**, 7639–7650.

44 Y. Hikichi, Y. Mori, S. Ishikawa, K. Hayashi, K. Ohnishi, A. Kiba and K. Kai, Regulation Involved in colonization of intercellular spaces of host plants in *Ralstonia solanacearum*, *Front. Plant Sci.*, 2017, **8**, DOI: 10.3389/fpls.2017.00967.

45 R. P. Garg, J. Huang, W. Yindeeyoungyeon, T. P. Denny and M. A. Schell, Multicomponent transcriptional regulation at the complex promoter of the exopolysaccharide I biosynthetic operon of *Ralstonia solanacearum*, *J. Bacteriol.*, 2000, **182**, 6659–6666.

46 G. Murtaza, A. Sajjad, Z. Mehmood, S. H. Shah and A. R. Siddiqi, Possible molecular targets for therapeutic applications of caffeic acid phenethyl ester in inflammation and cancer, *J. Food Drug Anal.*, 2015, **23**, 11–18.

47 S. M. Brumbley, B. F. Carney and T. P. Denny, Phenotype conversion in *Pseudomonas solanacearum* due to spontaneous inactivation of PhcA, a putative *LysR* transcriptional regulator, *J. Bacteriol.*, 1993, **175**, 5477–5487.

48 D. Aldon, B. Brito, C. Boucher and S. Genin, A bacterial sensor of plant cell contact controls the transcriptional induction of *Ralstonia solanacearum* pathogenicity genes, *EMBO J.*, 2014, **19**, 2304–2314.

